The Influence of Pacific-North American Teleconnection on the North Pacific SST Anomalies in Wintertime under the Global Warming

Zheng Chen (chenzhengouc@163.com)
Ocean University of China https://orcid.org/0000-0002-8727-8595
Bolan Gan
Ocean University of China
Fei Huang
Ocean University of China
Jianping Li
Ocean University of China
Lixin Wu
Ocean University of China
Lei Fan
Ocean University of China
Yina Diao
Ocean University of China

Research Article

Keywords: Global warming, Pacific Decadal Oscillation, Pacific-North American teleconnection, CMIP5 climate models

Posted Date: May 26th, 2022

DOI: https://doi.org/10.21203/rs.3.rs-1619127/v1

Abstract

The impact of the enhancing Pacific-North American teleconnection (PNA) on the intensity of the first mode of SST anomalies (SSTa) in wintertime North Pacific [known as the Pacific decadal oscillation (PDO)-like SST pattern] under global warming is studied using reanalysis datasets and 12 selected CMIP5 models. The robust observational result of the PNA one month ahead of the PDO shows that the PNA has a great effect on the PDO-like SSTa. The intensities of PNA and PDO are defined with elimination of ENSO effect to evaluate the direct impact of PNA on the PDO in North Pacific under global warming. By comparing RCP8.5 and historical scenario of selected multi-models (PNA enhanced models), future projection illustrates that the PDO intensity will intensify 2.2 times its internal variability. Approximately 67% of the increase in PDO variations is contributed by the PNA-induced SSTa in the future warming scenario of multi-models ensemble mean. Models with stronger intensification of PNA variability tends to have larger magnitude of SSTa response in the North Pacific, which has more contributions to the enhancement of PDO intensity change in a warmer climate. This may shed some light on the projection of PDO variability and the relative role of PNA forcing under the global warming.

1. Introduction

The dominant pattern of observed sea surface temperature (SST) variability in the wintertime North Pacific is referred to as the Pacific decadal oscillation (PDO), which has been first introduced by Mantua et al. (1997) as the leading empirical orthogonal function (EOF) of North Pacific (20°N–70°N) SST anomalies. The PDO is defined as departures from the climatology after removing the global mean SSTs, with characteristic time scales in the observed record of 15–25 year and 50–70 year (Minobe 1997). Figure 2a shows the observed PDO pattern for the years 1900–2012 from HadISST dataset (Rayner et al. 2003). The positive spatial pattern is featured with a “horseshoe” shape, with below-normal SSTa in the central North Pacific and the opposite SSTa along the west coast of North American and the eastern tropical Pacific.

The PDO has great climatic influences on the Pacific Rim. Positive PDO phases are associated with less precipitation and warmer air temperature anomalies in the northwestern and central America, and more precipitation and cooler air temperature anomalies in the southwestern America (Mantua and Hare 2002). The negative phase of the PDO is exactly opposite influences to the positive phase. Such influences have drawn attentions on its changes under the future global warming.

Numerous researches focus on the PDO on a decadal time scale, and it is mainly provided by the westward ocean Rossby wave propagation along the KOE region, which is the most important contributor to the decadal component of PDO, although the relative importance of propagation is different in different models (Zhang and Delworth 2015). The meridional displacement of the subtropical and subpolar gyre boundary generates the KOE SST anomaly. The positive SST anomalies can feed back to the overlying atmosphere, resulting high SLP anomalies that can further enhance initial SST anomalies via anomalous Ekman transport. This positive air–sea feedback over the North Pacific makes great

contributions to the decadal time scale and it is in agreement with observations (e.g., Seager et al. 2001; Nakamura and Kazmin 2003; Frankignoul and Sennéchael 2007; Zhang et al. 2011).

Teleconnections between the tropics and extratropics have an integrating effect on the PDO variability (Gu and Philander 1997; Schneider et al. 1999). Due to the sensitivity of North Pacific SSTa to the high-frequency atmospheric variability (Pierce et al. 2001; Newman et al. 2003), the ENSO induced teleconnection such as the Pacific-North America (PNA) teleconnection originated from the tropical Pacific makes efforts in the North Pacific by ocean-atmosphere interactions (Latif and Barnett 1994, 1996).

The PNA is a prominent mode of planetary-scale atmospheric variability over the North Pacific basin in boreal winter, which has powerful influences on the hydroclimate of the North Pacific rim. These dynamical changes are expected to impact the surface climate of North America especially in winter (e.g., Wallace and Gutzler 1981; Leathers et al. 1991; Nigam 2003).

Furthermore, the PNA's signature on the Aleutian Low is closely related to PDO (e.g., Latif and Barnett 1996; Deser et al. 2004). In addition, the PNA play an active role in connecting climate variabilities over the tropical and extratropical Pacific. On one hand, the El Niño-Southern Oscillation (ENSO) variability influences the surface climate over the North Pacific Rim through the atmospheric PNA-like changes (Alexander et al. 2002).

Based on the multi-model outputs of CMIP5, we have found that the North Pacific center of PNA on Aleutian Low will be enhancing under global warming (Chen et al., 2018). In this case, how PDO responses to the enhancing PNA in North Pacific is our interest.

The purpose of this study is to examine the changes in the PDO's spatial structure under global warming and its consequent change in the relationship with enhancing PNA intensity for the future projection. We also briefly discuss the effects of PNA on PDO in winter and the possible dynamical processes behind the amplitude change of PDO variation under global warming.

The paper is organized as follows. Section 2 describes the observational datasets, multi-model outputs and analysis methods. The 21st-century projected changes of PDO and the relative role of the enhancing PNA to drive significant PDO intensity change under global warming are shown in section 3. Summary and discussion is given in section 4.

2. Datasets And Methods

2.1 Observations and multi-model outputs

To investigate the observed PDO and the oceanic anomalies forced by PNA, we employ SST data taken from the Met Office Hadley Centre Sea Ice and Sea Surface Temperature version 1 (HadISST1) dataset, with a horizontal resolution of 1°×1° (Rayner et al. 2003). This dataset has been checked against other

reanalysis datasets (such as COBE, ERSST) and found relatively minor differences both in time series and pattern of PDO from the years 1901–2014 (Newman et al. 2016). The PNA index and its spatial pattern in observation are investigated based on geopotential height (GPH) from the Twentieth-Century Reanalysis dataset version 2c (20CRv2c), with a horizontal resolution of 2°×2° and 24 vertical pressure levels (Compo et al. 2011).

To explore the SST response to intensified PNAb (the deepen trough of positive PNA pattern located in the North Pacific) under global warming, we select 12 CMIP5 models (Table 1) in which the PNAb is found enhanced robustly (Chen et al. 2018), organized by the Program for Climate Model Diagnosis and Intercomparison for IPCC AR5 (Taylor et al. 2012). The multi-model outputs of CMIP5, including monthly GPH and SST are used for analysis. The pre-industrial (PI) control simulation represents the unforced natural variability of ocean-climate system with CO_2 concentration fixed at 280–290 ppm; the historical simulation indicates the observed oceanic and atmospheric composition changes in the 20th century; the future climate simulation under the Representative Concentration Pathways (RCP) 8.5 shows the worst global warming scenario, with the radiation forcing reaching approximately $8.5\mathrm{W}\mathrm{m}^{-2}$ in 2100 (equivalent to CO_2 concentration > 1370 ppm). To ensure that data comparison, we choose 95 years of data in historical simulation (1911–2005) and RCP8.5 scenario (2006–2100) to represent the past and future climate, respectively. Only one member (“r1i1p1”) run for each model is used in this study.

Table 1
List of 12 selected CMIP5 models analyzed in this study.

Institution, Country	Model Name	Spatial resolution of AGCM (lon×lat)
Commonwealth Scientific and Industrial Research Organisation and Bureau of Meteorology, Australia	ACCESS1.3	1.875°×1.25°
GCESS, BNU, China	BNU-ESM	2.8°×2.8°
Canadian Centre for Climate Modelling and Analysis, Canada	CanESM2	2.8°×2.8°
NSF/DOE National Center for Atmospheric Research Boulder, USA	CESM1(CAM5)	1.25°×0.9°
Centro Euro-Mediterraneo per i Cambiamenti Climatici, Italy	CMCC-CESM	3.75°×3.75°
NOAA Geophysical Fluid Dynamics Laboratory, USA	GFDL-CM3	1.25°×2°
	GFDL-ESM2G	1.25°×2°
National Institute of Meteorological Research, South Korea	HadGEM2-AO	1.875°×1.25°
	HadGEM2-ES	1.875°×1.25°
Institut Pierre Simon Laplace, France	IPSL-CM5A-LR	3.75°×1.875°
Max Planck Institute for Meteorology, Germany	MPI-ESM-LR	1.875°×1.875°
Norwegian Climate Centre, Norway	NorESM1-ME	2.5°×1.875°

In section 3, we use SST and GPH from the historical and RCP8.5 simulation of 12 selected models that exhibit the enhancement of PNAb to compare the PDO pattern between the two scenarios. These outputs are also employed to further investigate the projected future SST response to PNA forcing and its contribution to the intensity change of PDO.

2.2 PDO pattern and PNA forced SSTa along with their intensity

Previous studies have defined the PDO as the leading empirical orthogonal function (EOF) of the monthly averaged SST anomalies of North Pacific (e.g., Mantua et al. 1997; Newman et al. 2016). In this study, the observed PDO pattern is extracted by regressing SST anomalies on the normalized leading principal component (PC) of the North Pacific (20°-70°N), which represents the typical amplitude of PDO (i.e., one standard deviation of index). Note that the SST field is weighted by the square root of the cosine of latitude to account for the decrease of grid area poleward. In order to measure the intensity of PDO, all of the PDO patterns are adjusted to their positive phase, and the central North Pacific domain for the SST anomalies is set as a box (11° in latitude and 21° in longitude) centered on the pole of PDO minimum (as shown in Fig. 2a). The absolute area-averaged value of regression coefficients in the box is defined as the PDO intensity. Meanwhile, the PNA pattern and intensity are defined as the same in Chen et al. (2018). It

is also well known that the North Pacific atmosphere–ocean system fluctuates with periods of 2–7 years in response to El Niño–Southern Oscillation (ENSO) events(e.g., Bjerknes 1969; Horel and Wallace 1981; Rasmusson and Wallace 1983; Halpert and Ropelewski1992). And its associate PNA teleconnection cause changes in the North Pacific surface heat fluxes, Ekman transport and wind-driven mixing which all effect PDO pattern (Alexander et al. 2002; Alexander and Scott 2008; Strong and Magnusdottir 2009). Consider this circumstance, we use partial least squares (PLS) regression method to eliminate the ENSO effects and focus on the SST changes forced by PNA in the midlatitude. The PNA-forced SSTa pattern is calculated by PLS regressing SSTa on the PNA index and removing Niño 3.4. As the same with the PDO intensity, the PNA-forced SSTa intensity is computed by absolute area-averaged value of the identical domain (i.e., magenta boxes in Fig. 2e).

The PDO and PNA-forced SSTa pattern are calculated for the historical run and the RCP8.5 run separately, and their difference in intensities indicate the response to greenhouse warming. It is noted that the multi-model ensemble mean (MEM) statistics are calculated as the mean of the individual statistic being analyzed. For example, the MEM pattern of PDO is computed as the mean of individual patterns in positive phase which are derived by the regression of SSTa field onto the normalized PDO index from individual models.

2.3 Estimation of unforced internal variability in CMIP5 models

To test the significance of the projected PDO variability changes under greenhouse warming, we calculate the unforced internal variability of both modes based on the PI run of each model. First, we construct 41 segments with time increment of 95-yr, for which the starting year of each one was taken 10-yr apart from the 500-yr long (after spin-up) outputs of the PI run. These 41 segments are considered independent of each other under the assumption that atmospheric states among different segments are uncorrelated. Then, a total of 41 PDO patterns are derived from 41 segments. Indeed, further inspection finds no significant correlations of PDO index between two consecutive segments. Finally, we calculate the intensity of each PDO pattern, and the standard deviation of intensities across 41 patterns is used to measure the unforced internal variability of PDO. Also the unforced internal variability of PNA-forced SSTa pattern is calculated with the same method.

3. Results

3.1 The response of PDO to PNA in observation and model simulation

To measure the observed North Pacific SST variability generated by PNA, we first use the seasonal cycle of cross correlation between PDO (HadISST1 dataset) and PNA (20CRv2c dataset) monthly expansion coefficient (EC) time series (both are filtered with 3-month running mean, Fig. 1b). The observed correlations show that atmospheric variations generally lead SST variations (e.g., Davis 1976; Deser and

Timlin 1997). The springtime PDO has a high correlation with prior wintertime PNA variability. The maximum correlation value appears between January PNA and February SST, indicating that the PNA during its dominating season has a strong influence on the North Pacific SST variability in the later month. To confirm how dose PDO with a 1-month delay (JMF) change by PNA forcing in wintertime (DJF), we calculate the regression of the Pacific SSTa (30°S-70°N, 110°E-60°W) in JFM onto the observed PNA index in DJF (as shown in Fig. 2c). Unless otherwise noted, the season is fixed on DJF for atmospheric field and JFM for oceanic field through the paper. The regression pattern is similar to the observed PDO pattern (Fig. 2a), except for the weaker amplitude in SST variation. Note that the tropical Pacific SSTa excites atmospheric Rossby wave trains during ENSO events which force extratropical large-scale atmospheric teleconnections (e.g., Trenberth et al. 1998; Liu and Alexander 2007). And the PDO-like SST variations are effected by ENSO as well. Figure 1a shows that the observed PDO and ENSO index (here, defined as the Niño 3.4 index) are simultaneously correlated throughout the year. The high correlations at the lags from − 6 to 6 suggest significant interactions between ENSO and PDO. These results indicate that the ENSO signal entangles in both PNA and PDO signals.

To illustrate the PNA-induced SST variations, the PLS regression is employed to eliminate the ENSO effect (Fig. 2e). To further inspect the relationship between the PDO and the PNA-forced SSTa, we compare the time evolution of the intensities of the North Pacific center of the PDO (defined as the absolute regression coefficients averaged over the box in Fig. 2a) and the PNA-forced SSTa (the same as the former, but in Fig. 2e) as shown in Fig. 1c. The time evolutions of the intensities are constructed over 33 80-yr sliding windows (i.e., 1901–1980, 1902–1981, …, 1933–2012). The red (blue) line represents the time evolution of the North Pacific center intensity of the PDO (PNA-forced North Pacific SSTa). Here the time evolution of PNAb (the North Pacific center of PNA) intensity (green line in Fig. 1c) is constructed using the same methods as in Chen et al. (2018). The results show a robust connection between PDO and PNA-forced SSTa (Corr. =0.76, p = 0.01). Also PNAb and PDO reveal the significant correlations 0.69 with p-value 0.02. Percentages in black at the lower right corner of the graphs indicate the contribution of PNA-forced SSTa to PDO intensity, which is defined as $\mathrm{P} = \left(\sum_i^n |x_i| \,/\, \sum_i^n |y_i| \right) \bullet r \times 100\%$, where $x_i\left(y_i\right)$ is the PNA-forced SSTa (PDO) intensity in the i-th year and r is the correlation coefficient between these two variables. For example, if P reaches 100%, which means the variable x is exactly the same as y (there is no energy loss from x to y) and x is the only factor to cause the change of variable y. It shows that the wintertime PNA affects the North Pacific SST within one month, and it impacts on the PDO variability via the PNA-forced North Pacific SSTa.

Similar phenomenon also appears in the patterns (Fig. 2b, d, and f) of multi-model ensemble mean (MEM, see Table 1 for the details of the selected models), which demonstrate the model capability to simulate the observed atmospheric and oceanic variability in the tropical and North Pacific. When compared with the observe patterns, the amplitudes in Alaska Current area are overestimated for all the MEM patterns of Fig. 2. Besides that, the SST variations in Kuroshio Extension are also over-amplification in multi-model simulation (Fig. 2b), which may affect the position of the North Pacific center of PDO. In this case, we

avoid the Kuroshio Extension area and set the maximum value of SSTa as the North Pacific center of PDO in each selected CMIP5 model (as shown in Fig. 3).

3.2 Projected future changes of PDO and the contribution of PNA under global warming

Based on the statistics of PDO patterns in CMIP5 models, we find that the location of the North Pacific center is different from model to model. Thus we choose variable boxes to accommodate the different locations of the North Pacific center in different models. For all of the 12 models except the HadGEM2-ES model, the pattern difference between the RCP8.5 and historical scenario (Fig. 3) show an enhancement of the North Pacific center of the PDO under the global warming consistently. Besides, the overestimated Kuroshio Extension variability becomes weaker than historical scenario except NorESM1-ME model.

To measure the magnitude of the North Pacific SST response to the intensification of PNA under the warming scenario, the historical PLS regression pattern of each model along with the pattern difference between the RCP8.5 and Historical scenarios are drawn in Fig. 4. The multi-model collectively shows the PDO-like SSTa response under the forcing of PNA. However, the inter-model diversity promotes us to design tailored box for each model to measure the intensities of PNAb and its forced SSTa centers. Most of the selected models present good performance and show enhanced PNA-forced SSTa centers.

We have confirmed in our previous study that the PNA in these 12 models are enhanced in RCP8.5 scenario as well (also shown by the dashed lines of Fig. 4). The central location of PNAb in each model is denoted in the green box, and the PNAb intensity is defined as the area-averaged regression coefficients in that box.

The PNA-forced SSTa of the models only contribute to the negative (positive) value of SSTa in the North Pacific (Alaska Current). We use the same location (magenta boxes) as the PDO center to measure the intensity of the PNA-forced SSTa. The intensities differences between RCP8.5 and Historical scenario are calculated for PNAb (green bars), PDO (red bars) and PNA-forced SSTa (blue bars), as shown in Fig. 5. It suggests that the intensities of the North Pacific center of the PDO and the PNA-forced SSTa are intensified under global warming in models with enhanced PNAb except the HadGEM2-ES model. The projected change is considered significant when the magnitude exceeds the unforced internal variability which is measured based on the PI-control run. All the changes have passed significance test except PNA-forced SSTa change in CMCC-CESM model. Note that most of the intensity changes are more than twice the internal variability, but the only model (HadGEM2-ES) with a weakened PDO shows that the PNAb and the PNA-forced SSTa intensity changes are close to their internal variability. In general, through the numerical statistics of the North Pacific SSTa variability, the PDO will intensify in a warming climate and the enhancement of the PNA-forced SSTa is the main cause.

Although the enhancement of the North Pacific center of PDO in future projection (RCP8.5 scenario) is robust in the multiple models, the difference between individual models is primarily in magnitude. A

naturally raised issue is, to what extent the inter-model differences in the North Pacific center of PDO are related to the PNA variability and associated SST responses.

As shown in Fig. 6, we find a close inter-model relationship among the intensity changes of the PDO, the PNAb and the PNA-forced SSTa in multi-model projections. For these three variables, we examined the correlations between them, which are 0.78, 0.75, and 0.8, which are all significant at the 0.01 significance level. The MEM of the PDO intensity change shows an increase of 0.13°C with the 95% confidence interval of 0.06°C to 0.20°C (Fig. 6a), and the signal-to-noise ratio (i.e., change value divided by the estimation of unforced internal variability) is 2.22. Such an intimate linkage also holds for the MEM result, which shows an increase of 0.10°C with the 95% confidence interval of 0.05°C to 0.15°C (Fig. 6c), and the signal-to-noise ratio is 3.59. Meanwhile the enhanced PNA in warming projection also shows an increase of 11.74 gpm with the 95% confidence range of ± 2.71 gpm, and the signal-to-noise ratio is 2.8. Apparently, the changes among the future projections of the selected models will enhance consistently. High correlations with the models indicate little difference in the inter-model diversity. It gives us a robust conclusion on the cause of the PDO enhancement under global warming. The deepened trough of the PNAb will force a PDO-like SSTa pattern, and thus enhance the PDO.

3.3 Possible mechanism of the changes in North Pacific SSTa

To further inspect the evolution of the PDO intensity enhancement and the contribution of the PNA-forced SSTa to it under global warming, we examine the relationship between the North Pacific center of PDO and the PNA-forced SSTa with their projected intensity changes. The time evolution of the PDO intensity is constructed over 107 95-yr sliding windows (i.e., 1900–1994, 1901–1995, …, 2006–2100). Here the PDO intensity in each sliding window is derived from the area-averaged absolute regressions coefficients of the specific 95-yr late winter (JFM) SSTa against the PDO index in the selected boxes (the same boxes as in Fig. 3). Likewise, the time evolution of PNA and the PNA-forced SSTa intensity are calculated based on the area-averaged absolute regressions of winter (DJF) 500-hPa GPHa and JFM SSTa against the normalized PNA indices in the respective green and magenta boxes (Fig. 4) of each model. Note that similar results are obtained when using larger boxes. Here the statistical significance of correlation coefficient between the time series based on 95 years sliding window is tested with a two-tailed Student's t-test using the effective sample size, which takes into account the serial autocorrelation (Bretherton et al. 1999). The effective sample size (N_e) is defined as $N_e = N \times (1 - r_x \times r_y) / (1 + r_x \times r_y)$, where N is the length of time series and r_x(r_y) is the autocorrelation coefficient of the time series for variable x (y) at lag one.

As shown in Fig. 7, the MEM result clearly illustrates that the long-term evolution of the North Pacific center of PDO is in line with that of the PNA and the PNA-forced SSTa. All the intensities are increased gradually, particularly from 2030 and onward. It is obvious that there is a close association between the multidecadal evolution of the PDO intensity and PNA-forced SSTa, with high correlation coefficient of 0.96 at 0.01 significance levels. Also the PDO intensity has a close relationship with the PNAb intensity

(correlation coefficient 0.93). Note that the time coverage of the RCP8.5 data of CMCC-CESM is up to the year 2095 while that of the other models are all up to the year 2100, and the MEM timeline adjust to the shortest one. The definition of the percentages at the lower right corner of the graphs are the same as in Fig. 1c (see Sect. 3.1 for details)..

Figure 7 shows that all models except HadGEM2-ES can capture the close relationship between the time evolutions of the PDO North Pacific center intensity and the PNA along with its forced SSTa intensity. It is notable that PDO intensity is more correlated to the PNA-forced SSTa than it is to PNA. The percentage of contribution in each model ranges from 46.3–72.8%. Therefore, the PNA and the North Pacific SSTa forced by it will indeed intensify with global warming, and the PNA contributes about 67% of the intensification of PDO intensity.

Overall, the above results suggest that, on average, models with stronger intensification of PNA variability tend to have larger magnitude of PNA-forced SSTa response, which contributes more to the enhancement of PDO in a warmer climate.

4. Summary And Discussion

This study explores the relative roles of PNA in the long-term changes of PDO under global warming. The observational reanalysis and selected CMIP5 outputs have been analyzed. The former is for understanding the relationship between PNA and PDO variations. The latter simulates similar temporal and spatial features to that of the observation, and is employed to study the changes of PNA and its effects on PDO in a warming environment. The main findings are summarized as follows:

a. The wintertime PNA variability leads PDO variations by one month with a high correlation coefficient above 0.6. It suggests that the PNA during its dominating season (DJF) has a strong influence on the North Pacific SST variability in JFM for the thermal inertia of the ocean. The CMIP5 models simulate similar spatial features of PNA and PDO pattern to the observation. Note that the simulation of PNA shows a stronger North America ridge and a weaker North Pacific trough than observation, while the simulated PDO pattern shows higher amplitude in Alaska current area and Kuroshio Extension than observation.
b. The 12 selected CMIP5 models which PNAb intensities are increasing in future projection (Chen et al. 2018) perform well in simulating atmospheric and oceanic variability. By comparing RCP8.5 and historical scenario of each model, we find that 11 out of 12 models exhibit significant changes of PDO intensity and 10 out of 12 models show robust changes of PDO-like SSTa forced by PNA consistently in North Pacific under global warming. Specifically, the North Pacific trough deepens about 11.47±2.71 m (the 95% confidence interval, the same with below) in the 21st century, which is 2.8 times the unforced internal variability and drives 0.1±0.05 °C enhancement in the amplitude of PDO-like SSTa variation. Note that the PDO intensity increases 0.13±0.07 °C in the future projection, which is 2.2 times internal variability (Fig. 5 and 6). It is indicated that the PNA-forced SSTa is one of

the main factor causing the enhancement of PDO. In addition, the models show that the changes of PDO, PNA and PDO-like SSTa forced by PNA are closely related to each other.

c. The evolution of the PDO intensity is ever-increasing in the 21st century. In the North Pacific, the PNAb and the PNA-forced PDO-like SSTa also show enhancement in the future projection. The intensification of PDO-like SSTa forced by PNA is closely related to the intensification of PDO from early 21-st century onward. The contribution of the PNA-forced SSTa to the PDO intensification is 67.3% in the future projection, which is greater than that in the observation (50.7%). This may indicate a closer bond between the PNA and the PDO under global warming.

Overall, the above results suggest that, on average, models with stronger intensification of PNA variability tend to have larger magnitude of its associated SSTa response, which contributions to the enhancement of PDO in a warmer climate. A possible mechanism of this phenomenon is that the enhanced PNA causes larger wind anomalies which leads to an evaporation increase in the North Pacific center, and thus decreases the SST causing the larger amplitude of SSTa. This may shed some light on the projection of PDO changes and the role of the PNA in it under the global warming.

Declarations

Acknowledgements

We acknowledge the WCRP's Working Group on Coupled Modelling, which is responsible for CMIP, and we thank the climate modeling groups for producing and making available their model output. This work was supported by National Key Research and Development Program of China (2017YFA0603801, 2019YFA0607004), National Natural Science Foundation of China (NSFC) Projects (42006017, 41922039), Natural Science Foundation of Shandong Province (ZR2019BD038, ZR2019ZD12), Taishan Pandeng Scholar Project.

References

1. Alexander MA, Blade I, Newman M, Lanzante JR, Lau NC, Scott JD (2002) The atmospheric bridge: the influence of ENSO teleconnections on air-sea interaction over the global oceans. J Clim 15:2205–2231
2. Alexander MA, Scott JD (2008) The role of Ekman ocean heat transport in the Northern Hemisphere response to ENSO. J Clim 21:5688–5707
3. Bjerknes J (1969) Atmospheric teleconnections from the equatorial Pacific. Mon Wea Rev 97:163–172
4. Chen Z, Gan B, Wu L, Jia F (2018) Pacific-North American teleconnection and North Pacific Oscillation: historical simulation and future projection in CMIP5 models. Clim Dyn 50:4379–4403
5. Compo GP, Whitaker JS, Sardeshmukh PD, Matsui N, Allan BJ, YinX, Gleason BE, Vose RS, Rutledge G et al (2011) The twentieth century reanalysis project. Q J Roy Meteorol Soc 137:1–28

6. Davis RE (1976) Predictability of sea surface temperature and sea level pressure anomalies over the North Pacific Ocean. J Phys Oceanogr 6:249–266
7. Deser C, Timlin M (1997) Atmosphere–ocean interaction on weekly timescales in the North Atlantic and Pacific. J Clim 10:393–408
8. Deser C, Phillips AS, Hurrell JW (2004) Pacific interdecadal climate variability: Linkages between the tropics and the North Pacific during boreal winter since 1900. J Clim 17:3109–3124
9. Frankignoul C, Sennéchael N (2007) Observed influence of North Pacific SST anomalies on the atmospheric circulation. J Clim 20:592–606
10. Gu D, Philander SGH (1997) Interdecadal climate fluctuations that depend on exchanges between the tropics and extratropics. Science 275:805–807
11. Halpert MS, Ropelewski CF (1992) Surface temperature patterns associated with the Southern Oscillation. J Clim 5:577–593
12. Horel JD, Wallace JM (1981) Planetary-scale atmospheric phenomena associated with the Southern Oscillation. Mon Wea Rev 109:813–829
13. Latif M, Barnett TP (1994) Causes of decadal climate variability over the North Pacific and North America. Science 266:634–637
14. Latif M, Barnett TP (1996) Decadal climate variability over the North Pacific and North America: Dynamics and predictability. J Clim 9:2407–2423
15. Leathers DJ, Yarnal B, Palecki MA (1991) The Pacific/North American teleconnection pattern and United States climate. Part I: Regional temperature and precipitation associations. J Clim 4:517–528
16. Liu Z, Alexander MA (2007) Atmospheric bridge, oceanic tunnel and global climatic teleconnections. Rev Geophys 45:RG2005
17. Mantua NJ, Zhang Y, Wallace JM, Francis RC (1997) A Pacific interdecadal climate oscillation with impacts on salmon production. Bull Amer Meteor Soc 78:1069–1079
18. Mantua NJ, Hare SR (2002) The Pacific decadal oscillation. J Oceanogr 58:35–44
19. Minobe S (1997) A 50–70 year climatic oscillation over the North Pacific and North America. Geophys Res Lett 24:683–686
20. Nakamura H, Kazmin AS (2003) Decadal changes in the North Pacific oceanic frontal zones as revealed in ship and satellite observations. J Geophys Res 108:3078
21. Newman M, Compo GP, Alexander M (2003) ENSO-forced variability of the Pacific decadal oscillation. J Clim 16:3853–3857
22. Newman M, Alexander MA, Ault TR, Cobb KM, Deser C, Di Lorenzo E, Mantua NJ, Miller AJ, Minobe S, Nakamura H, Schneider N, Vimont DJ, Phillips AS, Scott JD, Smith CA (2016) The Pacifc decadal oscillation, revisited. J Clim 29:4399–4427
23. Nigam S (2003) Teleconnections. In: Holton JR, Pyle JA, Curry JA (eds) Encyclopedia of atmospheric sciences. Academic, London, pp 2243–2269

24. Pierce DW (2001) Distinguishing coupled ocean–atmosphere interactions from background noise in the North Pacific. Prog Oceanogr 49:331–352
25. Rasmusson EM, Wallace JM (1983) Meteorological aspects of the El Niño/Southern Oscillation. Science 222:1195–1202
26. Rayner NA, Parker DE, Horton EB, Folland CK, Alexander LV, Rowell D, Kent EC, Kaplan A (2003) Global analyses of sea surface temperature, sea ice, and night marine air temperature since the late nineteenth century. J Geophys Res 108:4407
27. Schneider N, Miller AJ, Alexander MA, Deser C (1999) Subduction of decadal North Pacific temperature anomalies: Observations and dynamics. J Phys Oceanogr 29:1056–1070
28. Seager R, Kushnir Y, Naik NH, Cane MA, Miller J (2001) Wind-driven shifts in the latitude of the Kuroshio–Oyashio extension and generation of SST anomalies on decadal timescales. J Clim 14:4249–4265
29. Strong C, Magnusdottir G (2009) The role of tropospheric Rossby wave breaking in the Pacific decadal oscillation. J Clim 22:1819–1833
30. Taylor KE, Stouffer RJ, Meehl GA (2012) An overview of CMIP5 and the experiment design. Bull Am Meteorol Soc 93(4):485–498
31. Trenberth KE, Branstator GW, Karoly D, Kumar A, Lau NC, Ropelewski C (1998) Progress during TOGA in understanding and modeling global teleconnections associated with tropical sea surface temperatures. J Geophys Res 103:14291–14324
32. Wallace JM, Gutzler DS (1981) Teleconnections in the geopotential height field during the northern hemisphere winter. Mon Weather Rev 109:784–812
33. Zhang L, Wu L, Zhang J (2011) Coupled ocean–atmosphere responses to recent freshwater changes over the Kuroshio Oyashio Extension region. J Clim 24:1507–1524
34. Zhang L, Delworth TL (2015) Analysis of the characteristics and mechanisms of the Pacific decadal oscillation in a suite of coupled models from the Geophysical Fluid Dynamics Laboratory. J Clim 28:7678–7701

Figures

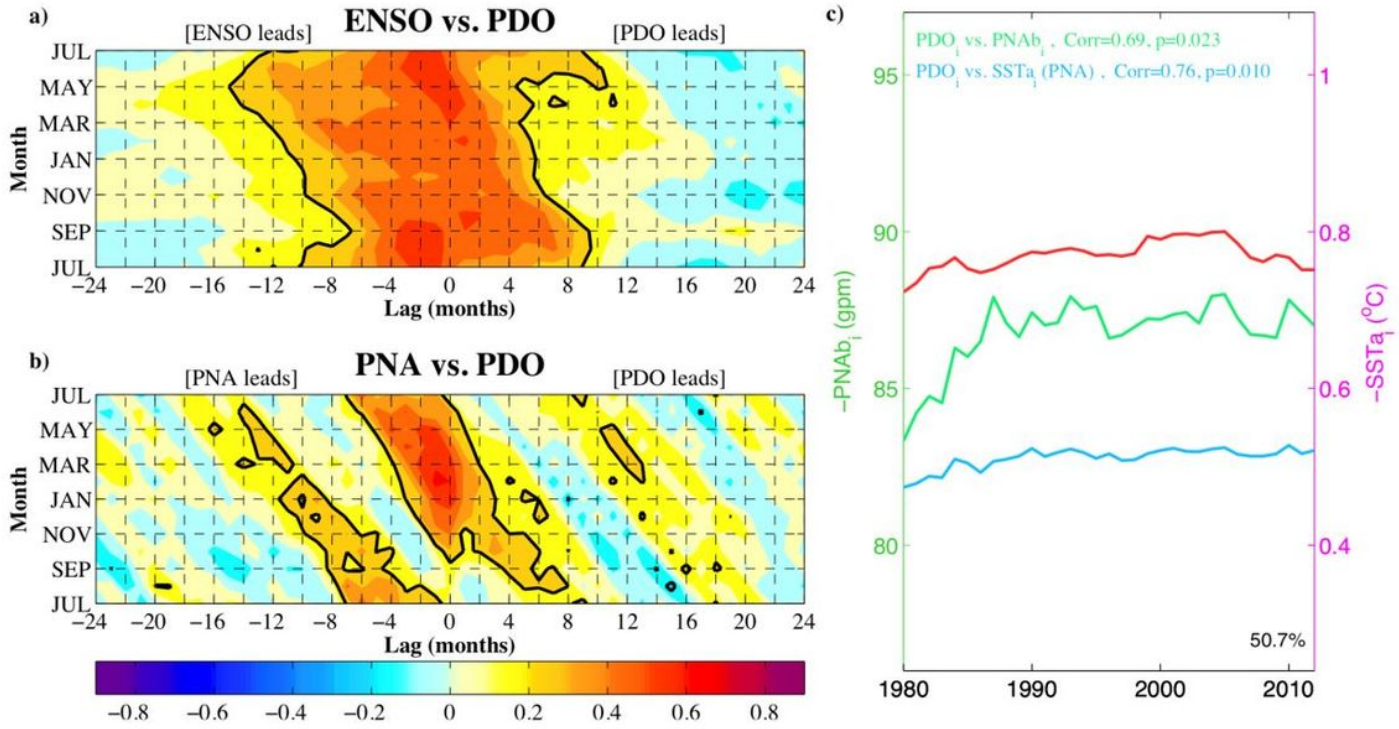

Figure 1

Illustration of how oceanic and atmospheric forcing can drive PDO variability. (a) Seasonal cycle of cross correlation between the Niño3.4 and PDO indices (both filtered with 3-month running mean). Positive (negative) lags are for PDO (ENSO) leading ENSO (PDO). (b) The same as in (a) but for PNA and PDO indices. In (a) and (b), both panels are determined from 1901-2012 data; shading interval is 0.1; black lines indicate values at the 0.05 significance level. The vertical axis indicates the month of the PDO index, and the horizontal axis indicates the lags (months) of PDO leading PNA. (c) Observed time evolution of the PDO intensity (red line; °C), PNAb intensity (green line; m) and the PNA-forced SSTa (blue line; °C) in winter after 80-year sliding window smoothing filtering. Correlation coefficient between the red line and the green (blue) line is shown in green (blue) color at the top, as well as the corresponding p value. The percentage at the lower right corner shows the contribution of PNA-forced SSTa to the PDO intensity change (see Sect. 3.1 for details). The years shown on the horizontal axis are the end years of the sliding windows.

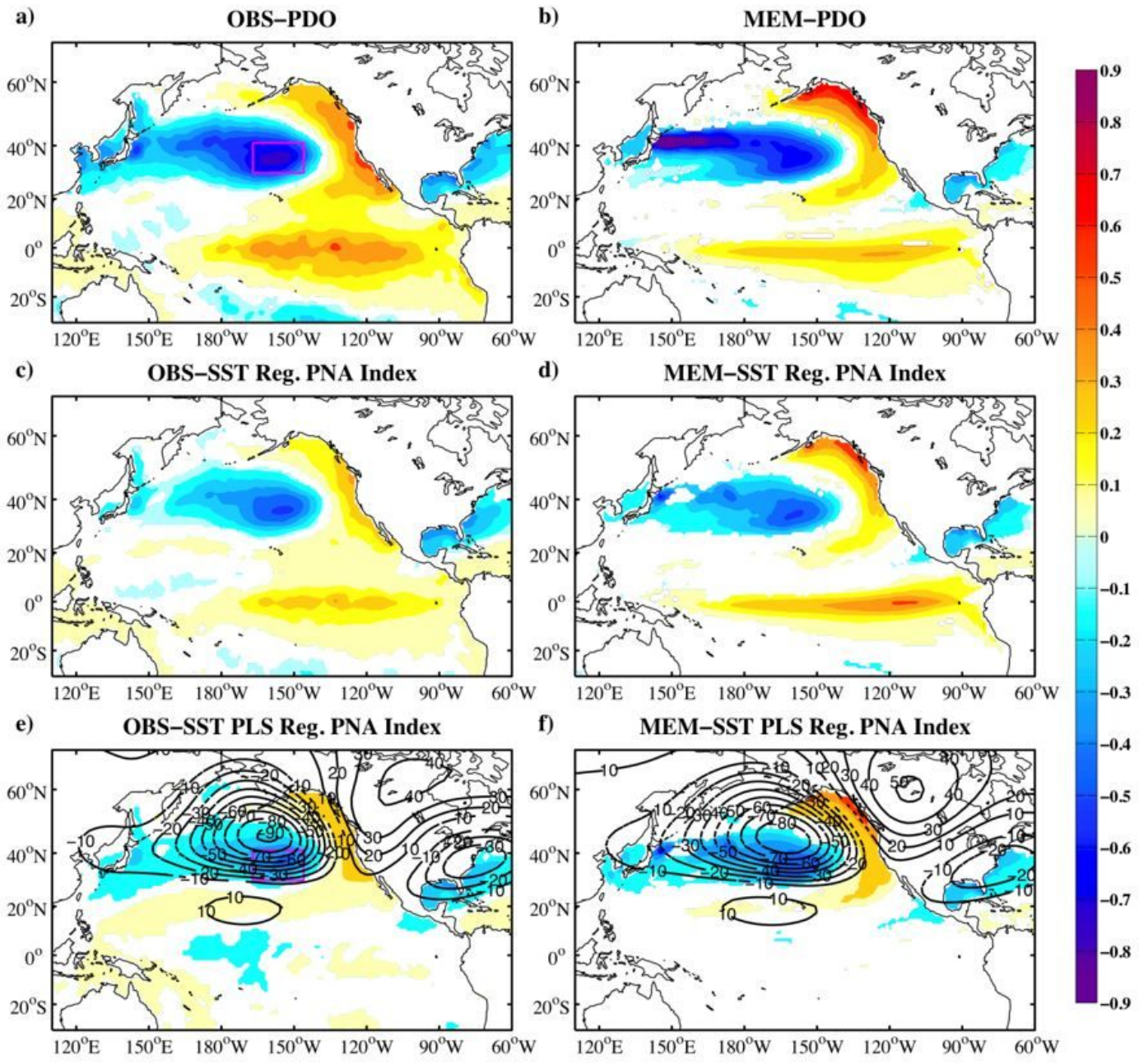

Figure 2

(a) Observed PDO pattern (°C) and (c) PDO-like SSTa regression pattern (°C) in winter corresponding to the normalized PC1 of 500-hPa GPHa. (e) PNA-forced SSTa pattern (°C) captured by removing ENSO effect. The PNA pattern in black dashed lines (unit: m) is corresponding to the normalized PC1 of 500-hPa GPHa. (b), (d), and (f) are as in (a), (c), (e), but for the ensemble-mean patterns of 12 selected models. Magenta boxes in (a) and (e) denote the domain used for the analysis in Fig. 1c.

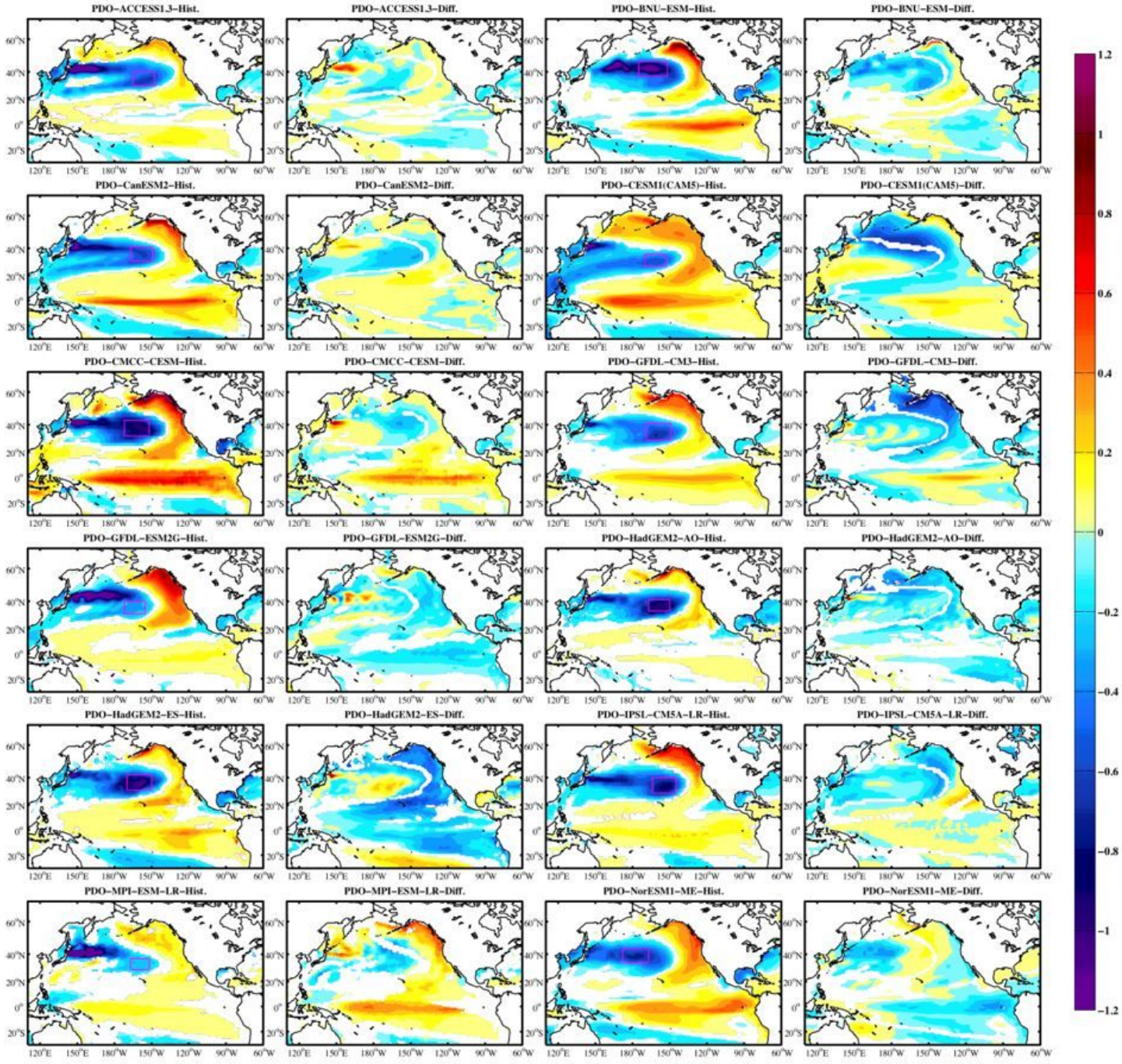

Figure 3

JFM PDO patterns (°C) in historical scenario of 12 selected models (the first and third columns). The shading area shows the regressions passing the 0.05 significance level test. The Magenta box of each model denotes the domain used for the analysis in Fig. 5-7. On the right of each historical PDO pattern is the difference of PDO patterns (°C) between the RCP8.5 and historical runs (RCP8.5 minus historical).

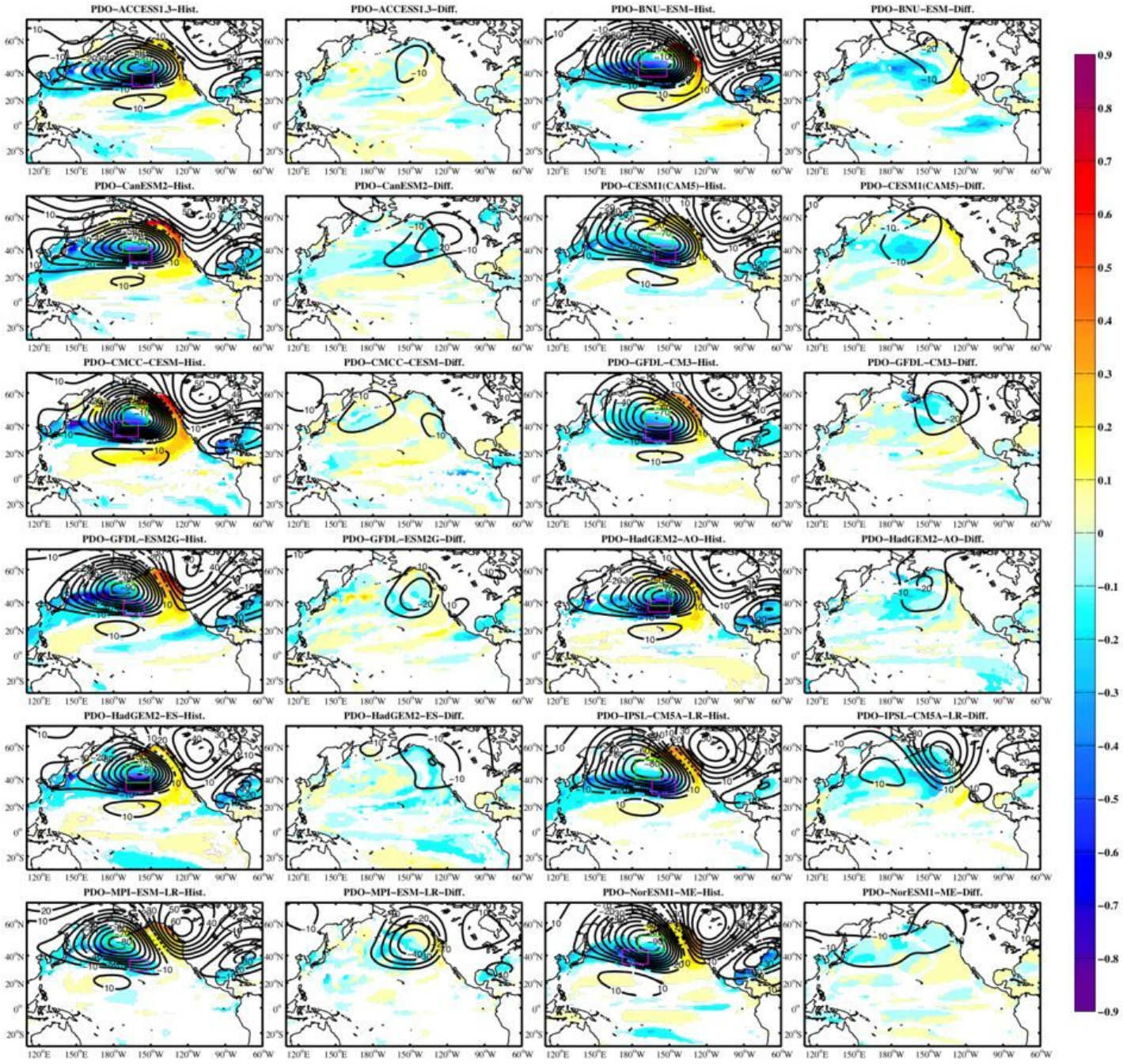

Figure 4

Similar to Fig. 3, but for the PNA-forced SSTa PLS regression patterns (°C), and also shown the PNA patterns [m; black solid (positive value) and dashed (negative value) line].

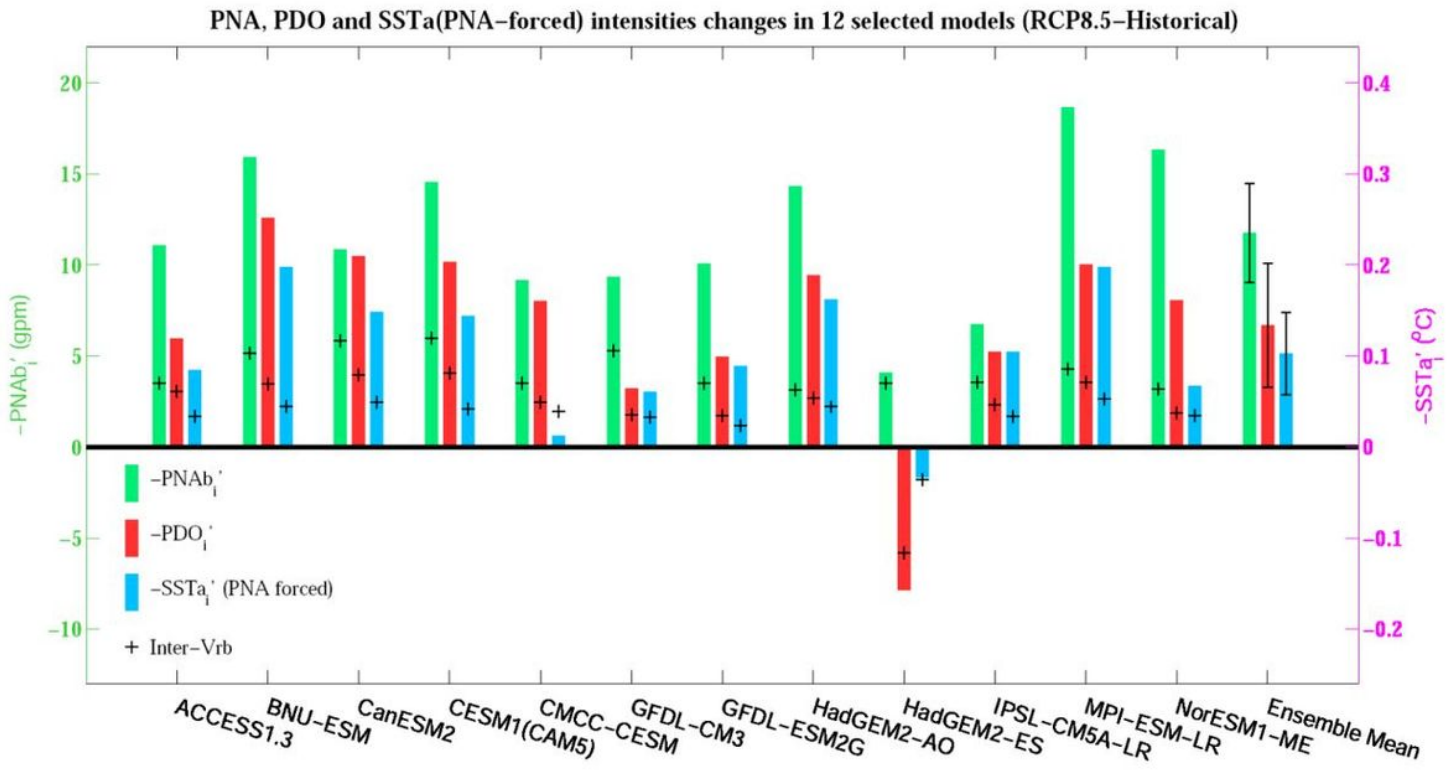

Figure 5

Changes in the intensities of PDO (°C), PNA (m) and PNA-forced SSTa (°C) in the central North Pacific from the historical scenario to the RCP8.5 scenario. See Sect. 2.2 for details on the definition of the intensity of both modes. The black "+" mark denotes the estimation of unforced internal variability based on the PI-control run. The error bars denote the 95% confidence interval based on a two-tailed Student's *t*-test. Note that the calculation is based on the absolute intensity of each variable, so that the positive (negative) value indicates the intensification (weakening).

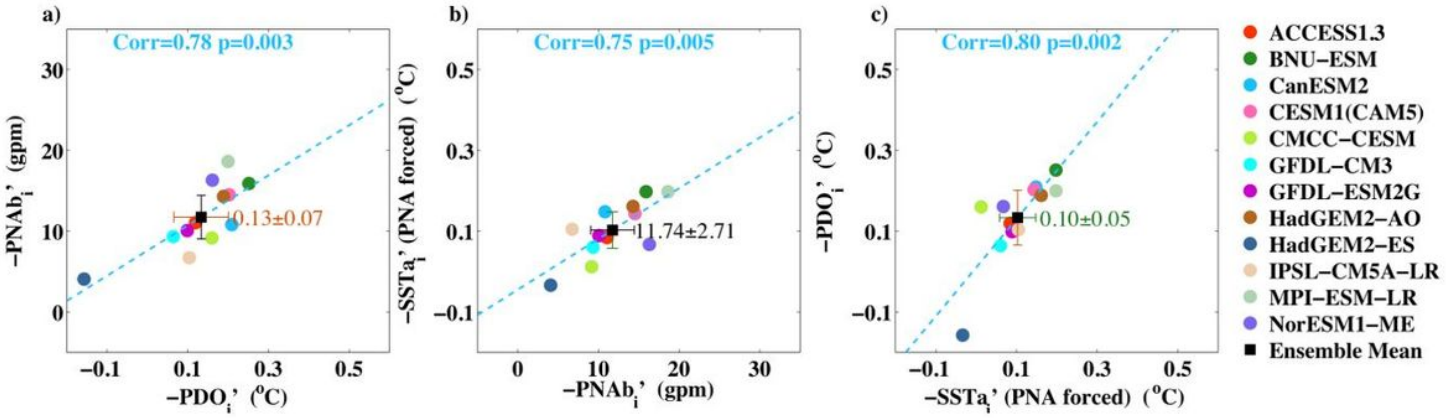

Figure 6

(a) Scatter diagram of the projected changes in the PDO intensity (°C, same as red bar in Fig. 5) versus changes in PNAb intensity (m, i.e. North Pacific trough, same as green bar in Fig. 5) across models. Changes are derived from the difference of 95-year-interval difference between the RCP8.5 and historical runs (RCP8.5 minus historical). The corresponding MEM and their uncertainties based on a two-tailed student's t test at the 95% confidence interval are indicated by a square with error bars, with nearby values showing for the three variables indicated on the horizontal axis. The projected change of the -PDO_i is 0.13 ± 0.07 °C. Blue lines denote the linear regression line, and the corresponding correlation coefficients and p values are shown at the top of each figure. (b) as in (a), but for the -$PNAb_i$ versus PNA-forced SSTa intensity (°C, same as blue bar in Fig. 5). The MEM projected change of -$PNAb_i$ is 11.74±2.71 m. (c) as in (a), but for the PNA forced SSTa (projected change is 0.10±0.05 °C) versus PDO intensity.

Figure 7

Time evolution of the absolute PDO intensity (red line corresponding to right vertical axis; °C), PNAb intensity (green line corresponding to left vertical axis; m) and PNA-forced SSTa intensity (blue line corresponding to right vertical axis; °C) in winter over 95-yr sliding windows from 1900 to 2100 for the MEM and individual models. Correlation coefficient between red line and green (blue) line is shown in green (blue) color, along with the corresponding p value. The percentage in black color at the lower right

corner shows the contribution of the PNA-forced SSTa to the change of PDO intensity (the same as in Fig. 1c). The last year of each sliding window is indicated on the horizontal axis.